

# Optical observations of the fast declining type Ib supernova iPTF13bvn

Shubham Srivastav<sup>\*</sup>, G. C. Anupama<sup>†</sup>, D. K. Sahu<sup>‡</sup>

*Indian Institute of Astrophysics, Koramangala, Bangalore 560 034, India*

10 September 2014

## ABSTRACT

We present optical UBVRI photometry and medium resolution spectroscopy of the type Ib supernova iPTF13bvn, spanning a phase of  $\sim -13$  d to  $+71$  d with respect to  $B$ -band maximum. The post maximum decline rates indicate a fast decline with  $\Delta m_{15}(B) = 1.82$ . Correcting for a galactic extinction  $E(B - V)_{\text{MW}} = 0.045$  and host galaxy extinction of  $E(B - V)_{\text{host}} = 0.17$ , the absolute  $V$ -band magnitude peaks at  $M_V = -17.23 \pm 0.20$ . The bolometric light curve indicates that  $\sim 0.09 M_{\odot}$  of  $^{56}\text{Ni}$  was synthesized in the explosion. The earliest spectrum ( $-13$  d) shows the presence of He I 5876 Å feature at a velocity of  $\sim 15000 \text{ km s}^{-1}$ , which falls rapidly by the time the SN approaches the epoch of  $B$ -band maximum. The photospheric velocity near maximum light, as indicated by the Fe II 5169 Å feature, is  $\sim 9000 \text{ km s}^{-1}$ . The estimate for the  $^{56}\text{Ni}$  mass, together with the estimates for the ejected mass ( $M_{\text{ej}}$ ) and kinetic energy of the explosion ( $E_k$ ) indicate that iPTF13bvn is a low luminosity type Ib supernova, with a lower than average ejected mass and kinetic energy. Our results suggest that the progenitor of iPTF13bvn is inconsistent with a single Wolf-Rayet star.

**Key words:** supernovae: general - supernovae: individual: iPTF13bvn - galaxies: individual: NGC 5806

## 1 INTRODUCTION

Core-collapse Supernovae (CCSNe) are caused by the violent deaths of massive ( $> 8 M_{\odot}$ ) stars which have exhausted their nuclear fuel. Type Ib supernovae (SNe Ib) are a sub-class of the hydrogen deficient Stripped Envelope CCSNe, which are identified by the presence of optical He I lines in their spectra (see Filippenko 1997 for a review). The two plausible progenitor scenarios involve either a massive Wolf-Rayet star (Gaskell et al. 1986) which has lost most of its outer envelope either through mass transfer to a companion or through strong stellar winds; or a relatively lower mass progenitor in a close binary system, eg. Podsiadlowski, Joss & Hsu (1992); Nomoto, Iwamoto & Suzuki (1995); see Smartt (2009) for a review. SNe Ibc, and CCSNe in general show a rich diversity in their photometric and spectroscopic characteristics, unlike the fairly homogeneous sub-class of SNe Ia. The diversity in the observed properties of CCSNe is attributed to the diversity in the nature and properties of the progenitor, such as its mass, radius, metallicity, mass-loss rate, rotation etc.

SN 1987A was the first supernova whose progenitor was un-

ambiguously identified in pre-explosion images as a blue supergiant (Gilmozzi et al. 1987; Kirshner et al. 1987). Since then, several progenitors of type II-P SNe, the most common type of CCSNe, have been identified in pre-explosion images. However, a lot remains to be understood about the progenitors of Stripped Envelope CCSNe.

The discovery of iPTF13bvn was reported by the intermediate Palomar Transient Factory (iPTF) on June 16.24 UT in the host galaxy of NGC 5806 at a redshift of 0.005 (Cao et al. 2013a). The discovery magnitude of the transient was 18.0 in the  $R$ -band, at the position  $\text{RA} = 15^{\text{h}} 00^{\text{m}} 00^{\text{s}}.18$ ,  $\text{Dec} = +01^{\circ} 52' 53''.5$ . There was nothing at the position of the supernova on June 15.29 UT, up to a limiting magnitude of 21.0. Subsequently, it was classified as a young SN Ib on June 17.8 UT (Milisavljevic et al. 2013). Cao et al. (2013b) present early phase photometry and spectroscopy of iPTF13bvn and also report a possible progenitor identification within a  $2\sigma$  error radius of 8.7 pc using HST pre-explosion images. The absolute luminosity, color and inferred mass loss rate from radio data for this potential progenitor was found to be consistent with a single Wolf Rayet (WR) progenitor. Using stellar evolution models, Groh, Georgy & Ekström (2013) conclude that the properties of the candidate progenitor are consistent with that of a single WR star, in agreement with Cao et al. (2013b). However, based on early and late phase observations of iPT13bvn

<sup>\*</sup> E-mail : ssrivastav@iiap.res.in

<sup>†</sup> E-mail : gca@iiap.res.in

<sup>‡</sup> E-mail : dks@iiap.res.in

and hydrodynamic modeling of the bolometric light curve, Fremling et al. (2014) (hereafter F14) conclude that the bolometric light curve is inconsistent with a single WR star progenitor, as previously suggested by Cao et al. (2013b) and Groh et al. (2013). Further, Bersten et al. (2014) (hereafter B14) perform hydrodynamic modeling of the bolometric light curve and propose an interacting binary system as the progenitor for iPTF13bvn. B14 also predict that the remaining companion, which is likely to have O-type characteristics, could possibly be detected in the future with deep HST imaging once the supernova has faded sufficiently. Such a detection will provide the first confirmation for the interacting binary progenitor scenario for SNe Ibc.

In this paper, we present early phase optical photometry and spectroscopy of iPTF13bvn, followed by discussions based on the observed characteristics of the supernova.

## 2 DATA REDUCTION

### 2.1 Photometry

Photometric observations of iPTF13bvn commenced on 2013 June 18,  $\sim 13$  days before B-band maximum, using the 2-m Himalayan Chandra Telescope at the Indian Astronomical Observatory at Hanle, and continued till 2013 September 10. The observations were made with the Himalayan Faint Object Spectrograph Camera (HFOSC). The SITe CCD available with the HFOSC has an imaging area of  $2K \times 4K$  pixels, of which the central unvignetted  $2K \times 2K$  area was used for imaging. The field of view in imaging mode is  $10 \times 10$  arcmin<sup>2</sup>, with an image scale of  $0.296$  arcsec pixel<sup>-1</sup>. The supernova was imaged in the Bessell *UBVRI* filters available with the HFOSC. Landolt standard fields PG1633+099 and PG2213-006 (Landolt 1992) were observed under photometric conditions on the nights of 2013 July 13 and July 29 for photometric calibration of the supernova field.

Data reduction was performed in the standard manner using various packages available with the Image Reduction and Analysis Facility (IRAF<sup>1</sup>). Aperture photometry was performed on the standard stars at an optimal aperture, determined using the aperture growth curve method. An aperture correction was applied between the optimal aperture and an aperture close to the FWHM of the stellar profile. Average extinction coefficients for the site (Stalin et al. 2008) were used in order to account for atmospheric extinction and average values of the color terms for the HFOSC system were used to arrive at the photometric solutions. The solutions thus obtained were used to calibrate several local standards in the supernova field, observed on the same night as the standard fields. The local standards were thereafter used to estimate the supernova magnitudes. The magnitudes of the supernova and the secondary standards were evaluated using point-spread function (PSF) fitting, with a fitting radius close to the full width at half-maximum (FWHM) of the stellar profile. Nightly photometric zero points were estimated

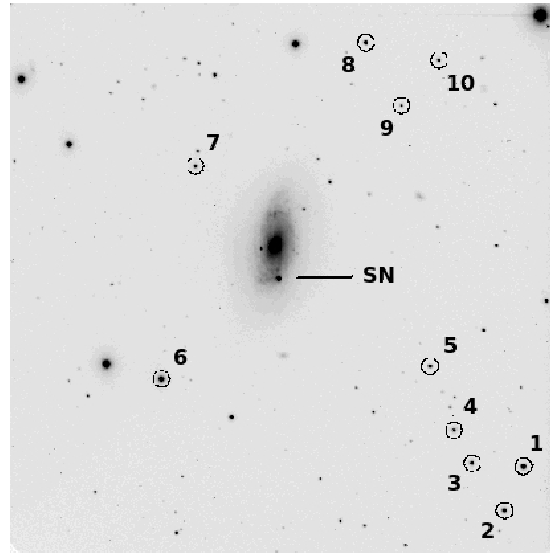


**Figure 1.** Identification chart for iPTF13bvn. North is up and East is to the left. The field of view is  $10' \times 10'$ . Local standards are marked.

using the local secondary standards and the supernova magnitudes were evaluated differentially.

The field for iPTF13bvn is shown in Figure 1, and the magnitudes of the secondary standards are listed in Table 1. Table 2 summarizes the photometric observations and magnitudes of iPTF13bvn.

### 2.2 Spectroscopy

Spectroscopic observations of iPTF13bvn were made on nine epochs during 2013 June 18 and 2013 Aug 06, using grisms Gr7 (3500-7800 Å) and Gr8 (5200-9250 Å) available with the HFOSC. The details of the spectroscopic observations are summarized in Table 3. Lamp spectra of FeAr and FeNe were used for wavelength calibration. The spectra were extracted in the standard manner. Night sky emission lines  $\lambda 5577$ ,  $\lambda 6300$  and  $\lambda 6363$  were used to check the wavelength calibration and spectra were shifted wherever necessary. Spectra of spectrophotometric standards were observed in order to deduce instrumental response curves for flux calibration. For those nights where standard star observations were not available, the response curves obtained during nearby nights were used. The flux calibrated spectra in grisms Gr7 and Gr8 were combined with appropriate scaling to give a single spectrum, which was brought to an absolute flux scale using the broadband *UBVRI* photometric magnitudes. The spectra were corrected for redshift of the host galaxy. The telluric lines have not been removed from the spectra.

## 3 OPTICAL LIGHT CURVES

iPTF13bvn was observed in Bessell *UBVRI* filters for a period spanning a phase of  $-13.1 d$  to  $+70.8 d$  with respect to *B*-band maximum. The epoch of maximum brightness and the peak magnitudes in each band were determined by fitting a spline curve through the points near maximum. The light curves in the bluer bands peak at earlier times. The

<sup>1</sup> IRAF is distributed by the National Optical Astronomy Observatories, which are operated by the Association of Universities for Research in Astronomy, Inc., under cooperative agreement with the National Science Foundation

**Table 1.** Magnitudes of secondary standards in the field of iPTF13bvn

ID	U	B	V	R	I
1	16.76 ± 0.03	16.25 ± 0.03	15.37 ± 0.03	14.83 ± 0.02	14.35 ± 0.01
2	18.26 ± 0.05	16.92 ± 0.03	15.63 ± 0.03	14.85 ± 0.02	14.18 ± 0.02
3	16.45 ± 0.03	16.62 ± 0.02	16.05 ± 0.02	15.67 ± 0.03	15.29 ± 0.02
4	16.95 ± 0.03	16.80 ± 0.02	16.09 ± 0.02	15.67 ± 0.02	15.28 ± 0.02
5	17.31 ± 0.04	17.42 ± 0.03	16.76 ± 0.02	16.33 ± 0.03	15.89 ± 0.03
6	15.10 ± 0.03				
7		17.07 ± 0.03	16.14 ± 0.02	15.55 ± 0.02	15.04 ± 0.02
8	17.28 ± 0.03				
9		17.48 ± 0.04	16.88 ± 0.03	16.48 ± 0.03	16.06 ± 0.03
10	17.49 ± 0.04	17.41 ± 0.03	16.68 ± 0.02	16.22 ± 0.03	15.76 ± 0.02

**Table 2.** Optical photometry of iPTF13bvn

Date	JD (245 6000+)	Phase* (days)	U	B	V	R	I
2013/06/18	462.14	−13.10		17.69 ± 0.02	16.93 ± 0.01	16.71 ± 0.01	16.58 ± 0.01
2013/06/19	463.13	−12.11		17.36 ± 0.02	16.69 ± 0.01	16.39 ± 0.01	16.26 ± 0.02
2013/06/21	465.05	−10.19		16.71 ± 0.02	16.19 ± 0.02	15.87 ± 0.03	15.84 ± 0.02
2013/06/22	466.14	−9.10		16.45 ± 0.03	15.99 ± 0.02	15.70 ± 0.01	15.63 ± 0.01
2013/06/25	469.22	−6.02	15.66 ± 0.03	15.95 ± 0.01	15.56 ± 0.01	15.33 ± 0.01	15.25 ± 0.02
2013/06/28	472.24	−3.00	15.64 ± 0.03	15.79 ± 0.01	15.37 ± 0.02	15.09 ± 0.01	14.97 ± 0.01
2013/06/30	474.12	−1.12	15.69 ± 0.02	15.78 ± 0.02	15.24 ± 0.01	15.01 ± 0.01	14.91 ± 0.02
2013/07/01	475.23	−0.01		15.77 ± 0.01	15.20 ± 0.01	14.93 ± 0.01	14.84 ± 0.01
2013/07/03	477.18	+1.94		15.83 ± 0.02	15.20 ± 0.01	14.91 ± 0.02	14.78 ± 0.01
2013/07/04	478.21	+2.97	15.99 ± 0.03	15.90 ± 0.02	15.23 ± 0.01	14.89 ± 0.01	14.75 ± 0.01
2013/07/10	484.27	+9.03		16.64 ± 0.01	15.62 ± 0.01	15.06 ± 0.04	14.89 ± 0.02
2013/07/11	485.22	+9.98		16.82 ± 0.01	15.73 ± 0.01	15.23 ± 0.01	14.99 ± 0.01
2013/07/12	486.16	+10.92			15.87 ± 0.01	15.37 ± 0.01	15.07 ± 0.01
2013/07/13	487.25	+12.01	17.79 ± 0.02	17.20 ± 0.01	15.99 ± 0.01	15.47 ± 0.01	15.15 ± 0.01
2013/07/20	494.18	+18.94		17.86 ± 0.02	16.57 ± 0.01	15.94 ± 0.01	15.53 ± 0.02
2013/07/23	497.12	+21.88		18.00 ± 0.02	16.73 ± 0.01	16.12 ± 0.01	15.74 ± 0.02
2013/07/29	503.16	+27.92	18.80 ± 0.03	18.19 ± 0.01	16.97 ± 0.01	16.33 ± 0.01	15.89 ± 0.01
2013/08/06	511.17	+35.93		18.22 ± 0.02	17.18 ± 0.02	16.55 ± 0.02	16.10 ± 0.03
2013/09/10	546.08	+70.84			17.82 ± 0.03	17.36 ± 0.03	

\* time since B-band max

**Table 3.** Log of spectroscopic observations of iPT13bvn

Date	JD 245 6000+	Phase (days)	Range (Å)
2013/06/18	462.16	−13.08	3500-7800; 5200-9250
2013/06/19	463.17	−12.07	3500-7800; 5200-9250
2013/06/25	469.24	−6.0	3500-7800; 5200-9250
2013/06/28	472.20	−3.04	3500-7800; 5200-9250
2013/07/01	475.24	+0.0	3500-7800; 5200-9250
2013/07/04	478.23	+2.99	3500-7800; 5200-9250
2013/07/11	485.23	+9.99	3500-7800; 5200-9250
2013/07/23	497.13	+21.89	3500-7800; 5200-9250
2013/08/06	511.19	+35.95	3500-7800; 5200-9250

supernova reached *B*-band maximum on JD 2456 475.24, at an observed apparent magnitude of  $15.77 \pm 0.02$ . The light curves are presented in Figure 2.

Using a power law model to fit the early *r*-band data for

iPTF13bvn, Cao et al. (2013b) suggest the explosion date as June 15.67 UT, which implies that the SN was detected within 1 day of the explosion. No signature of shock cooling was detected, however, unlike in the case of SN 2008D (Modjaz et al. 2009). Using this explosion date for iPTF13bvn, the rise time to maximum in the *B*-band is found to be  $\sim 16$  days, whereas the rise time for the redder bands is longer, as seen in Table 4. We use a rise time of 16 days in this work.

The light curves show a fast decline, with  $\Delta m_{15}(B) = 1.82$ . The post-maximum decline rates are higher than those of most SNe Ibc in the literature, a notable exception being SN 1994I (Richmond et al. 1996). The light curves of iPTF13bvn are compared with a few well-studied SNe Ibc like SN 2009jf (Sahu et al. 2011), SN 2007gr (Hunter et al. 2009), SN 2007Y (Stritzinger et al. 2009), SN 1999ex (Stritzinger et al. 2002) and SN 1994I (Richmond et al. 1996) in Figure 4. The reported magnitudes of SN 2007Y, which were in the *u*, *g*, *B*, *V* and *r* and *i* bands, were transformed to the *UBVRI* system us-

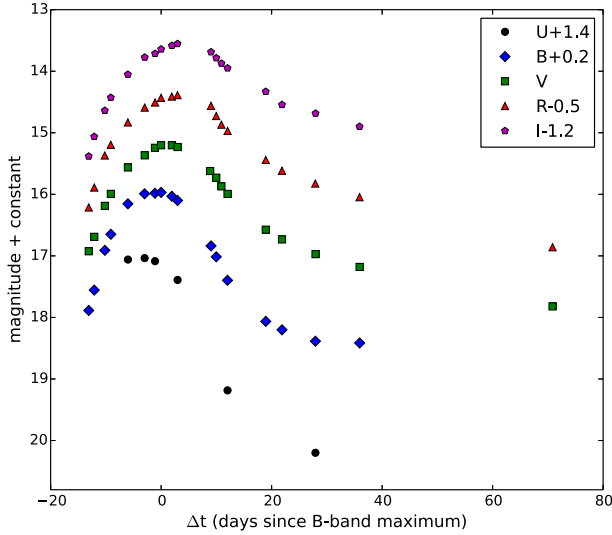


**Figure 2.** Optical light curves for iPTF13bvn. The light curves have been shifted for clarity by the amount as indicated in the legend. The errors in the SN magnitudes are within or comparable to the size of the markers.

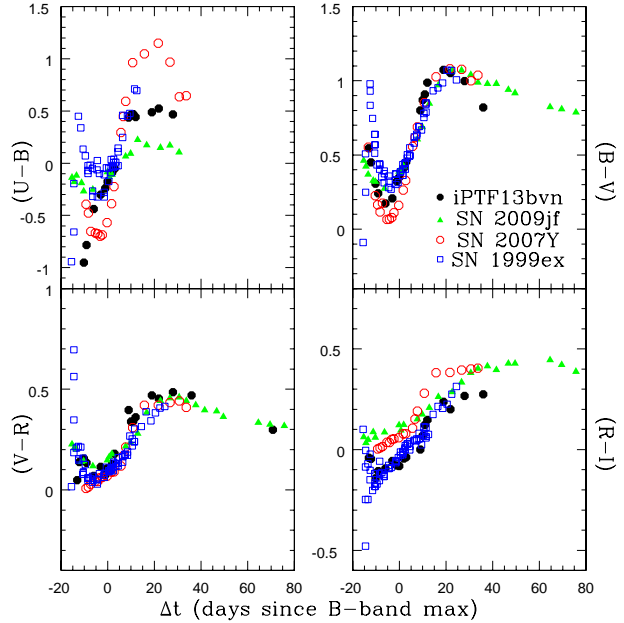


**Figure 4.** Color evolution of iPTF13bvn, plotted along with that of SN 2009jf, SN 2007Y and SN 1999ex. The extinction correction applied was  $E(B-V)_{\text{MW}} = 0.045$  and  $E(B-V)_{\text{host}} = 0.17$ , as discussed in Section 6.

towards blue in the pre-maximum phase. The  $(B-V)$  color reaches a minimum at  $\sim 5$  days before  $B$ -band maximum. Post maximum, the colors redden monotonically till  $\sim 20$  days past  $B$ -band maximum, beyond which the  $(B-V)$  color starts becoming bluer again, whereas the  $(V-R)$  and  $(R-I)$  colors remain more or less constant.

## 4 SPECTRAL EVOLUTION

Spectroscopic observations of iPTF13bvn were obtained on 9 epochs, starting from  $\sim 13$  days before  $B$ -band maximum up to  $\sim 36$  days past maximum.

### 4.1 Pre-maximum Spectra

The pre-maximum spectra (Figure 5) show broad P-Cygni profiles indicating a high expansion velocity of the ejecta. The first spectrum, obtained 13 days before  $B$ -band maximum, shows the presence of He I 5876 Å absorption feature at a velocity of  $\sim 15000 \text{ km s}^{-1}$ , with a possible contribution from Na I D 5890, 5896 Å. The He I 5876 Å velocity was reported to be  $\sim 16000 - 18000 \text{ km s}^{-1}$  by Milisavljevic et al. (2013) on June 17.8 UT, which corresponds to  $\sim 14$  days before  $B$ -band maximum.

The spectra show an early emergence of He I 5876 Å feature, similar to SN 2009jf (Sahu et al. 2011). Other prominent features in the first spectrum are identified as Mg II 4481 Å, Fe II lines (4555, 4924, 5018 Å), Si II 6355 Å, O I 7774 Å and the Ca II NIR triplet (8498, 8542, 8662 Å). The other features of He I at 4471, 5015, 6678, 7065 Å are weak in the first spectrum but gradually become stronger as the supernova evolves towards maximum light. The He I 7065 Å feature is affected by the telluric O<sub>2</sub> feature. The continuum

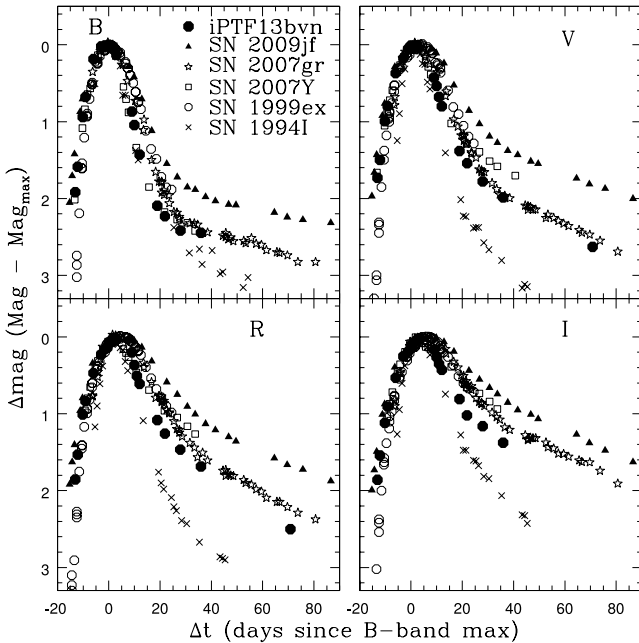


**Figure 3.** Comparison of BVRI light curves of iPTF13bvn, SN 2009jf, SN 2007gr, SN 2007Y, SN 1999ex and SN 1994I. The light curves have been shifted as described in the text.

ing the transformations prescribed by Jester et al. (2005). The magnitudes of the supernovae have been normalized to their respective peak magnitudes and the time axis has been shifted to the epoch of maximum brightness in the  $B$ -band. The decline rates for iPTF13bvn suggest that the light curves are similar, though slightly faster declining than those of the narrow-lined type Ic SN 2007gr.

The color evolution of iPTF13bvn is shown in Figure ?? . The  $(B-V)$ ,  $(V-R)$  and  $(R-I)$  colors of iPTF13bvn evolve

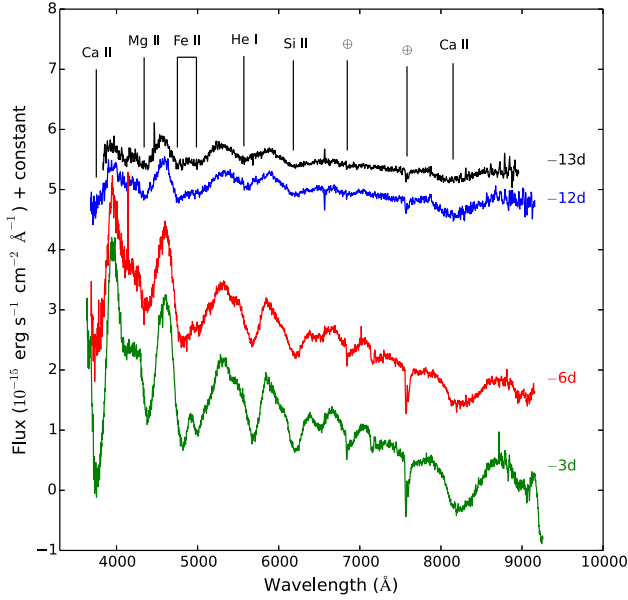


**Figure 5.** Spectral evolution in the pre-maximum phase for iPTF13bvn. The prominent features in the spectra are marked.

becomes bluer as the supernova approaches the epoch of *B*-band maximum, a trend also seen in the color evolution of the supernova.

The absorption trough at  $\sim 6200$  Å in the early spectra of SNe Ib is often attributed to a combination of photospheric Si II and/or high velocity ( $\gtrsim 15000$  km s $^{-1}$ ), detached H $\alpha$  (eg. Branch et al. 2002; Anupama et al. 2005; Folatelli et al. 2006; Parrent et al. 2007; Stritzinger et al. 2009; Tanaka et al. 2009). Using synthetic spectra generated with SYNOW, Elmhamdi et al. (2006) argue that traces of Hydrogen are present in most, if not all SNe Ib spectra. We identify the absorption trough at  $\sim 6200$  Å in the early spectra of iPTF13bvn as Si II 6355 Å. Cao et al. (2013b) suggest that the feature may also be associated with Ne I (eg. Benetti et al. 2002).

The pre-maximum spectra of SN iPTF13bvn are compared with those of SN 2009jf and SN 2007Y at similar epochs in Figure 6. iPTF13bvn shows remarkable similarity with SN 2009jf in the pre-maximum phase at similar epochs, although the  $-6$ d spectrum of iPTF13bvn shows a bluer continuum when compared to the  $-7$ d spectrum of SN 2009jf. In contrast to iPTF13bvn and SN 2009jf, the He I and Ca II NIR features in the early pre-maximum spectra of SN 2007Y are weak, but the Fe II features present in the 4000–5000 Å range are well developed.

#### 4.2 Post-maximum Spectra

The immediate post-maximum spectral evolution is shown in Figure 7. The spectrum obtained near maximum light exhibits a blue continuum and prominent signatures of He I, Fe II and Ca II. The He I features 5876, 6678 and 7065 Å exhibit different expansion velocities and a single velocity in the synthetic spectrum is unable to fit the ob-

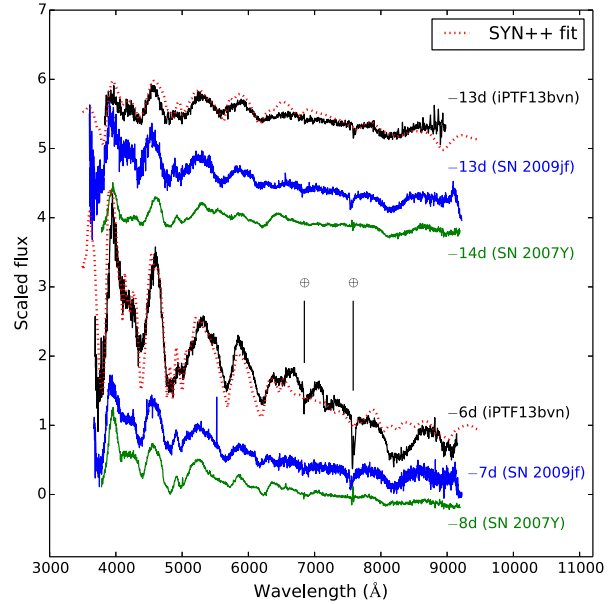


**Figure 6.** Comparison of pre-maximum spectra of iPTF13bvn with SN 2009jf and SN 2007Y.

served spectrum (F14, Cao et al. 2013b). The absorption trough near 6200 Å, which we associate with Si II 6355 Å weakens after maximum, and disappears beyond +10 days. A similar trend was seen for the Si II 6355 Å feature in the case of SN 2009jf (Sahu et al. 2011). The spectrum of iPTF13bvn obtained near maximum light is fit by a synthetic spectrum with photospheric velocity  $v_{\text{ph}} = 9000$  km s $^{-1}$  and effective blackbody temperature  $T_{\text{bb}} = 13000$  K, using SYN++. SYN++ is a modern C++ rewrite of SYNOW, the parameterized spectrum synthesis code (see Thomas, Nugent & Meza 2011; Fisher 2000). The spectrum obtained at +10 days is fit by a synthetic spectrum with reduced values of  $v_{\text{ph}} = 6500$  km s $^{-1}$  and  $T_{\text{bb}} = 6000$  K, which further reduce to  $v_{\text{ph}} = 5500$  km s $^{-1}$  and  $T_{\text{bb}} = 5000$  K to fit the +23 day spectrum.

The maximum light and immediate post-maximum spectra of iPTF13bvn are compared with those of SN 2009jf and SN 2007Y at similar epochs in Figure 8. The maximum light spectrum of iPTF13bvn shows a good match with SN 2009jf. At +10 days and beyond, the spectra of the three SNe look similar.

#### 5 EJECTA EXPANSION VELOCITIES

The expansion velocities of various features were deduced by fitting a Gaussian to the minimum of the absorption trough in the spectra corrected for the redshift of the host galaxy. A synthetic spectrum generated using SYN++, with a photospheric velocity of  $\sim 11000$  km s $^{-1}$  deduced from Fe II 5169 Å feature, fits the first spectrum obtained at phase  $-13$  days. The photospheric velocity decreases steadily, reaching  $\sim 9000$  km s $^{-1}$  at the epoch of *B*-band maximum and dropping further to below  $\sim 6000$  km s $^{-1}$  around 20 days past

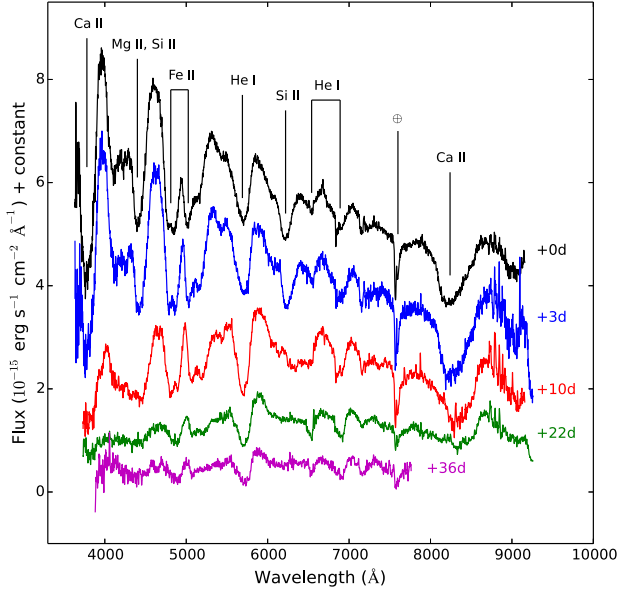


**Figure 7.** Spectral evolution in the immediate post-maximum phase for iPTF13bvn.

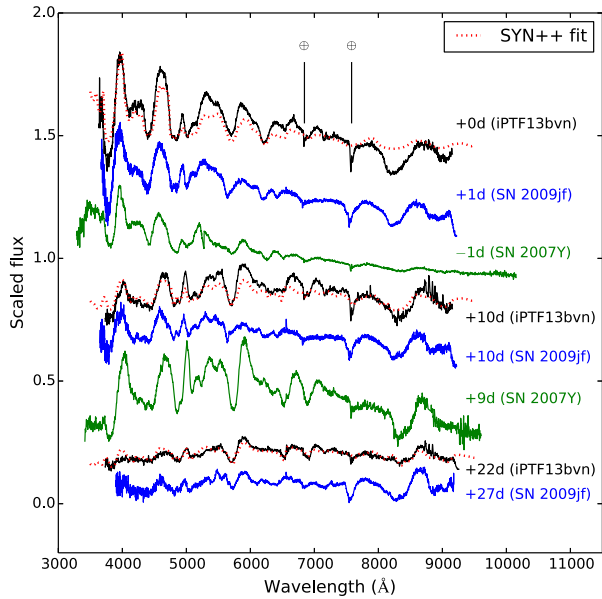


**Figure 8.** Comparison of immediate post-maximum spectra of iPTF13bvn with SN 2009jf and SN 2007Y. The dotted lines are the SYN++ fits to the spectra of iPTF13bvn.

maximum. The He I 5876 Å shows a velocity of  $\sim 15000 \text{ km s}^{-1}$  at  $-13$  days, which drops down rapidly to  $\sim 9500 \text{ km s}^{-1}$  near the epoch of maximum light, and further falls to  $\sim 8300 \text{ km s}^{-1}$  at a phase of  $+36$  days. The velocity evolution of the Ca II NIR triplet follows that of the He I 5876 Å feature, with a value of  $\sim 14000 \text{ km s}^{-1}$  at  $-13$  days but subsequently

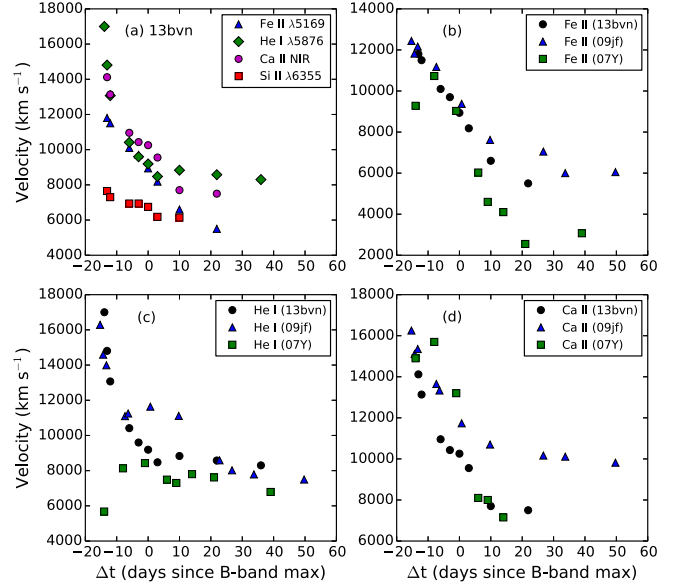


**Figure 9.** (a) Temporal evolution of velocity for the prominent features in the spectra of iPTF13bvn. (b), (c), (d) Comparison of Fe II 5169 Å, He I 5876 Å and Ca II NIR triplet velocities in iPTF13bvn with SN 2009jf and SN 2007Y.

settles to a lower velocity of  $\sim 7500 \text{ km s}^{-1}$  at  $+22$  days. The Si II 6355 Å feature has a relatively lower velocity of  $\sim 7500 \text{ km s}^{-1}$  at  $-13$  days, which falls to below  $6000 \text{ km s}^{-1}$  post maximum. The lower velocity of the Si II, compared to the photospheric velocity is probably due to mixing. Modeling results of B14 indicate a high level of mixing. A similar trend in velocity evolution was also seen in the case of SN 2009jf (Sahu et al. 2011) and SN 2007Y (Stritzinger et al. 2009). The measured velocities for iPTF13bvn are consistent with those reported by Cao et al. (2013b) and F14.

The velocity evolution of the He I 5876 Å feature for iPTF13bvn matches well with SN 2009jf, whereas that of SN 2007Y exhibits a lower velocity of  $\sim 8000 \text{ km s}^{-1}$  near maximum light. The evolution of the Fe II 5169 Å velocities in iPTF13bvn also matches with SN 2009jf till around maximum, beyond which it drops to a lower value. The velocity evolution of prominent features in the spectra of iPTF13bvn is shown in Figure 9, along with a comparison of the velocity evolution of Fe II 5169 Å, He I 5876 Å and Ca II NIR triplet with SN 2009jf (Sahu et al. 2011) and SN 2007Y (Stritzinger et al. 2009).

## 6 DISTANCE AND REDDENING

In order to correct for reddening, we adopt a galactic foreground extinction of  $E(B - V)_{\text{MW}} = 0.045$  in the direction of the host galaxy NGC 5806 (Schlafly & Finkbeiner 2011). Since SNe Ibc are associated with dusty star-forming regions (van Dyk, Hamuy & Filippenko 1996, Anderson & James 2008, Kelly, Kirshner & Pahre 2008), they typically suffer from significant host galaxy reddening. Using a sample consisting of 25 SNe Ibc, Drout et al. (2011) find that the



host galaxy reddening nearly always dominates the galactic foreground reddening, with an average host reddening of  $E(B - V)_{\text{host}} = 0.21 \pm 0.20$ . Combining their sample with those existing in the literature, Drout et al. estimate a mean host galaxy reddening of  $E(B - V)_{\text{host}} = 0.36 \pm 0.24$  for SNe Ibc.

Comparing the  $(B - V)$  color of iPTF13bvn with an intrinsic color law derived from a sample of SNe Ibc, B14 estimate  $E(B - V)_{\text{host}} = 0.17 \pm 0.03$ . On the other hand, Cao et al. (2013b) provide a much lower value of  $E(B - V)_{\text{host}} = 0.044$ , deduced from the equivalent width of Na I D lines in high resolution spectra. This difference in the host reddening estimates is significant, corresponding to  $\Delta A_V = 0.39$ , considering a standard reddening law (Cardelli, Clayton & Mathis 1989) with  $R_V = 3.1$ .

Drout et al. (2011) suggest using the color evolution of SNe Ibc as an independent indicator for the line of sight reddening. Specifically, the scatter in the extinction-corrected  $(V - R)$  color curves is reported to be minimum at  $\sim 10$  days after maximum in  $V$  and  $R$  bands, with mean values of  $\langle (V - R)_{V10} \rangle = 0.26 \pm 0.06$  and  $\langle (V - R)_{R10} \rangle = 0.29 \pm 0.08$ . For iPTF13bvn,  $(V - R)_{V10} = 0.43$  and  $(V - R)_{R10} = 0.38$  for  $E(B - V)_{\text{host}} = 0.044$ ; whereas  $(V - R)_{V10} = 0.34$  and  $(V - R)_{R10} = 0.29$  for  $E(B - V)_{\text{host}} = 0.17$ . In the latter case, the  $(V - R)$  values of iPTF13bvn are closer to the mean values suggested by Drout et al. (2011). Thus, the color evolution favors a host reddening of  $E(B - V)_{\text{host}} = 0.17$ . In the following analysis, we use  $E(B - V)_{\text{host}} = 0.17$  for iPTF13bvn.

Adopting a distance modulus  $\mu = 31.76 \pm 0.36$  (Tully et al. 2009), which yields a distance of  $22.49^{+4.06}_{-3.44}$  Mpc, the estimated peak absolute magnitude in the  $B$  and  $V$  bands is  $-16.88 \pm 0.20$  mag and  $-17.25 \pm 0.20$ , respectively. Table 4 lists the estimated peak absolute magnitudes in the  $UBVRI$  bands. The errors in the absolute magnitudes were estimated taking into account the photometric errors on the observed magnitudes and the error in the distance modulus.

## 7 BOLOMETRIC LIGHT CURVE

The quasi-bolometric light curve for iPTF13bvn was constructed by converting the extinction corrected broadband  $UBVRI$  magnitudes to monochromatic fluxes using the zero points from Bessell, Castelli & Plez (1998). A spline curve was then fit through the monochromatic fluxes and the resulting curve was integrated under appropriate limits of wavelength as determined from the filter response curves, to yield the quasi-bolometric flux for the particular epoch. Since  $U$ -band observations are not available beyond phase +28, we use only the  $BVRI$  magnitudes to estimate the bolometric flux thereafter. The quasi-bolometric light curve is plotted in Figure 10, along with the bolometric light curves of SN 2009jf, SN 2007gr, SN 2007Y, SN 1999ex and SN 1994I for comparison. The quasi-bolometric light curves of SN 2009jf (Sahu et al. 2011), SN 2007gr (Hunter et al. 2009), SN 2007Y (Stritzinger et al. 2009), SN 1999ex (Stritzinger et al. 2002) and SN 1994I (Richmond et al. 1996) were constructed in a similar manner using the published  $UBVRI$  magnitudes. A total reddening  $E(B - V)$  of 0.112, 0.092, 0.11, 0.3 and 0.45 was adopted and distances were assumed to be 34.66, 29.84, 19.31, 48.31 and

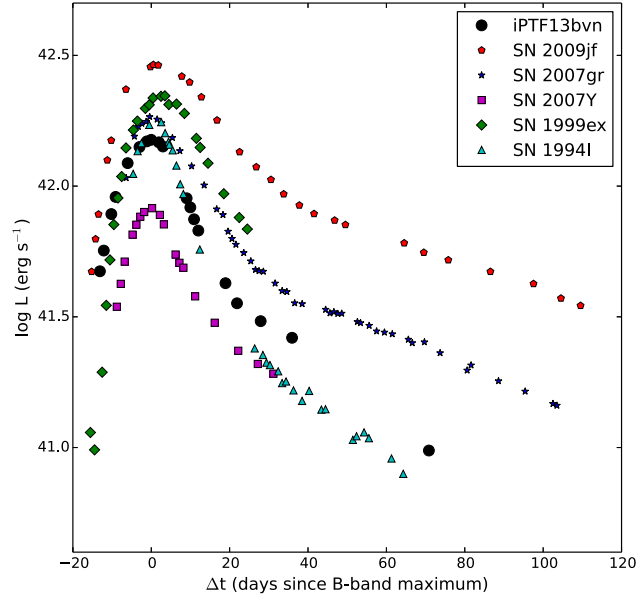


**Figure 10.** Bolometric light curve of iPTF13bvn, plotted along with bolometric light curves of SN 2009jf, SN 2007gr, SN 2007Y, SN 1999ex and SN 1994I for comparison.

8.32 Mpc for SN 2009jf, SN 2007gr, SN 2007Y, SN 1999ex and SN 1994I, respectively.

Assuming the date of explosion to be June 15.67 UT (Cao et al. 2013b), the bolometric light curve rises to a peak in  $\sim 16$  days. With a peak bolometric magnitude of  $-16.76 \pm 0.20$  (for  $E(B - V)_{\text{host}} = 0.17$ ), iPT13bvn is  $\sim 0.8$  mag brighter than the SN Ib 2007Y,  $\sim 0.20$  mag fainter than SNe Ic 1994I and 2007gr, and  $\sim 0.7$  mag fainter than the normal SN Ib 2009jf. The radioactive tail of the bolometric light curve (past 60 days of explosion) shows a fast decline rate of  $3 \text{ mag } 100 \text{ d}^{-1}$ , which is much higher than the theoretically expected rate of  $0.98 \text{ mag } 100 \text{ d}^{-1}$  powered by the decay of radioactive  $^{56}\text{Co}$ . The fast decline indicates an optically thin ejecta with inefficient  $\gamma$ -ray trapping at later phases.

We note that the contribution of the Ultraviolet (UV) and Near Infrared (NIR) bands has not been included in the calculation of the bolometric light curve. For SN 2007Y, Stritzinger et al. (2009) found a UV contribution of  $\sim 20 \%$  and NIR contribution of  $\sim 5 \%$  at maximum light. However, by two weeks past maximum, the UV flux drops to  $\leq 10 \%$ , while the NIR contribution rises to  $\sim 20 \%$  of the total bolometric flux. Modjaz et al. (2009) report a NIR contribution of  $\sim 20 \%$  for SN 2008D near two weeks past maximum. Thus, the UV and NIR bands together can contribute  $\sim 30 \%$  of the bolometric flux at any given epoch.

**Table 4.** Peak magnitudes, decline rates and colors for iPTF13bvn

Filter	Phase at peak (days)	Decline Rate $\Delta m_{15}$	Peak apparent magnitude	Peak absolute magnitude $E(B - V)_{\text{host}} = 0.044$ $E(B - V)_{\text{host}} = 0.17$	
U	-3.77		$15.63 \pm 0.04$	$-16.56 \pm 0.19$	$-17.17 \pm 0.22$
B	0.00	$1.82 \pm 0.05$	$15.77 \pm 0.02$	$-16.36 \pm 0.17$	$-16.88 \pm 0.20$
V	+0.92	$1.16 \pm 0.04$	$15.19 \pm 0.02$	$-16.85 \pm 0.17$	$-17.25 \pm 0.20$
R	+5.64	$1.22 \pm 0.04$	$14.83 \pm 0.02$	$-17.12 \pm 0.17$	$-17.44 \pm 0.20$
I	+5.10	$0.90 \pm 0.04$	$14.72 \pm 0.02$	$-17.19 \pm 0.17$	$-17.38 \pm 0.20$
Color	$E(B - V)_{\text{host}} = 0.044$	$E(B - V)_{\text{host}} = 0.17$			
$(U - B)_{\text{Bmax}}$	-0.09	-0.18			
$(B - V)_{\text{Bmax}}$	0.48	0.35			
$(V - R)_{\text{Bmax}}$	0.21	0.11			
$(R - I)_{\text{Bmax}}$	0.02	-0.08			
$(V - R)_{V10}$	0.43	0.34			
$(V - R)_{R10}$	0.38	0.29			

## 8 PHYSICAL PARAMETERS OF THE EXPLOSION

A combination of three parameters, namely the mass of  $^{56}\text{Ni}$  synthesized in the explosion ( $M_{\text{Ni}}$ ), the total ejecta mass ( $M_{\text{ej}}$ ) and the kinetic energy of the explosion ( $E_k$ ) determines the peak luminosity and the width of the bolometric light curve (Arnett 1982). A higher peak luminosity indicates a larger value of  $M_{\text{Ni}}$ , and a larger ejecta mass results in broader light curves (Ensmann & Woosley 1988). The diffusion time  $\tau_m$ , which is a measure of the width of the bolometric light curve, is related to  $M_{\text{ej}}$  and  $E_k$  as  $\tau_m \propto \kappa^{1/2} M_{\text{ej}}^{3/4} E_k^{-1/4}$ , whereas the photospheric expansion velocity of the ejecta is related to  $M_{\text{ej}}$  and  $E_k$  as  $v_{\text{ph}} \propto \sqrt{E_k/M_{\text{ej}}}$  (see Arnett 1982).

Arnett's rule suggests that the mass of  $^{56}\text{Ni}$  synthesized in the explosion can be estimated by equating the peak bolometric luminosity with the instantaneous rate of radioactive decay. Nugent et al. (1995) proposed a simplified formulation of Arnett's rule to calculate the  $^{56}\text{Ni}$  mass,

$$M_{\text{Ni}} = \frac{L_{\text{bol}}^{\text{max}}}{\alpha \dot{S}}$$

Here,  $\alpha$  is the ratio of bolometric and radioactivity luminosity, whereas  $\dot{S}$  refers to radioactivity luminosity per unit nickel mass, which depends on the rise time to maximum. The quasi-bolometric luminosity of iPTF13bvn peaks at  $1.05^{+0.4}_{-0.4} \times 10^{42} \text{ ergs s}^{-1}$  (for  $E(B - V)_{\text{host}} = 0.044$ ) and  $1.50^{+0.4}_{-0.4} \times 10^{42} \text{ ergs s}^{-1}$  (for  $E(B - V)_{\text{host}} = 0.17$ ). The uncertainties in the peak flux are primarily due to the uncertainty in the distance modulus. Assuming a rise time of  $16 \pm 1$  days (Section 7), and  $\alpha$  to be unity, the mass of  $^{56}\text{Ni}$  is estimated to be  $0.05^{+0.02}_{-0.02} M_{\odot}$  and  $0.08^{+0.02}_{-0.02}$ , for  $E(B - V)_{\text{host}}$  values of 0.044 and 0.17, respectively.

In order to estimate the physical parameters of the explosion, such as  $M_{\text{Ni}}$ ,  $M_{\text{ej}}$  and  $E_k$ , we fit the observed quasi-bolometric light curve of iPTF13bvn with the simple analytical model proposed by Vinkó et al. (2004). This model assumes homologous expansion of the ejecta, and a constant opacity for  $\gamma$ -rays and positrons. A core-shell density structure is assumed, with a constant density core of fractional radius  $x_0$ , and a surrounding shell whose density decreases outward as a power law with exponent  $n$ . A short diffu-

sion time is assumed, which allows the emitted bolometric luminosity to be approximated as the rate of energy deposition. This assumption is however not valid during pre-maximum epochs when the ejecta is optically thick, and therefore this model is applied only to the post-maximum phase of the bolometric light curve. Following Vinkó et al. (2004), the time-dependent rate of energy deposition by  $\gamma$ -rays and positrons can be expressed as

$$\epsilon = E_{\gamma} (1 - \exp(-\tau_{\gamma})) + E_{+} (1 - \exp(-\tau_{+})),$$

where  $E_{\gamma}$ ,  $E_{+}$  are energy input rates from  $\gamma$ -rays and positrons, and  $\tau_{\gamma}$ ,  $\tau_{+}$  denote the optical depths for  $\gamma$ -rays and positrons respectively (Cappellaro et al. 1997), which in turn can be expressed as

$$\tau_{\gamma,+} = \kappa_{\gamma,+} \rho_0(t) R(t) x_0 \left(1 + \frac{1 - x_0^{n-1}}{n - 1}\right).$$

Here,  $\rho_0(t) = \frac{M_{\text{ej}}}{4\pi R(t)^3 f(x_0)}$  is the time-varying core density, where  $R(t) = v_{\text{exp}} t$  (homologous expansion) and  $f(x_0)$  is a geometrical factor due to the assumed density configuration. The kinetic energy of the explosion then becomes

$$E_k = \frac{3}{10} \frac{3 - n}{5 - n} \frac{5x_0^n - nx_0^5}{3x_0^n - nx_0^3} M_{\text{ej}} v_{\text{exp}}^2.$$

Vinkó et al. (2004) define three models based on the assumed density configuration characterized by  $x_0$  and  $n$ . Model A is a constant density model with  $n = 0$ , Model B is a power-law model with  $x_0 = 0.01$  and Model C is a core-shell model with  $x_0 = 0.15$ . The free parameters in the models are ejected mass ( $M_{\text{ej}}$ ), nickel mass ( $M_{\text{Ni}}$ ),  $\gamma$ -ray opacity ( $\kappa_{\gamma}$ ), positron opacity ( $\kappa_{+}$ ), expansion velocity ( $v_{\text{exp}}$ ) and the density power law exponent ( $n$ ).

Table 5 summarizes the best-fit values of the parameters and Figure 11 shows the results of the model fits to the bolometric light curve. The three models give similar results, with the models A and C fitting the observed data slightly better. The models favor a low value of the gamma-ray opacity ( $\kappa_{\gamma} < 0.01$ ), in contrast to the usual value of 0.027 for grey atmospheres (Sutherland & Wheeler 1984). The constant density model A yields slightly higher values of opacities, as also seen in the case of SN 2002ap (Vinkó et al. 2004). The above models assume spherical symmetry and



homologous expansion of the ejecta. However, owing to the binary nature of the progenitor (B14), the ejecta is likely to be aspherical. Therefore, the results tabulated in Table 5 should only be treated as an order-of-magnitude estimate of the parameters, as also noted by Vinkó et al. (2004). Defining an additional model C1 where the value of  $\kappa_\gamma$  is fixed at 0.027, the fit is found to be poorer (Fig 11). Fixing the  $\gamma$ -ray opacity in model C1 results in a model whose peak luminosity is too low, and late phase decline too slow to explain the observed bolometric light curve.

Hydrodynamic modeling of the bolometric light curve of iPTF13bvn requires  $^{56}\text{Ni}$  to be highly mixed in the outer layers of the ejecta (B14, F14). If the  $^{56}\text{Ni}$  is highly mixed,  $\gamma$ -ray escape commences earlier and the bolometric light curve is fainter and declines faster during the radioactive tail (Woosley et al. 1994). The He I features observed in SNe Ib spectra require nonthermal excitation caused by  $\gamma$ -rays emitted by the decay of  $^{56}\text{Ni}$  freshly synthesized in the explosion (Lucy 1991). The early emergence of the He I features in the spectra of iPTF13bvn indicates either a thoroughly mixed ejecta, or a small ejecta mass which would facilitate escape of  $\gamma$ -rays from the  $^{56}\text{Ni}$ -rich region, or both. Thus, a low ejecta mass and a significant amount of mixing of  $^{56}\text{Ni}$  can explain the fast decline of the late phase bolometric light curve and the preference for models with low  $\gamma$ -ray opacity.

We derive the physical parameters of the explosion as  $M_{\text{ej}} \sim 1.5 - 2.2 M_\odot$ ,  $M_{\text{Ni}} \sim 0.09 M_\odot$ ,  $E_{51} \sim 1.0$  erg (Table 5). Accounting for a 30 % (constant) contribution from missing passbands (UV and NIR) slightly raises these estimates to  $M_{\text{ej}} \sim 2 - 3 M_\odot$  and  $M_{\text{Ni}} \sim 0.12 M_\odot$ . These estimates are consistent with those of F14 ( $M_{\text{ej}} \approx 1.94 M_\odot$ ,  $M_{\text{Ni}} \approx 0.05 M_\odot$ ,  $E_{51} \approx 0.85$  erg) and B14 ( $M_{\text{ej}} \approx 2.3 M_\odot$ ,  $M_{\text{Ni}} \approx 0.1 M_\odot$ ,  $E_{51} \approx 0.7$  erg), derived from detailed hydrodynamic modeling of the bolometric light curve. F14 use a host extinction correction of  $E(B - V)_{\text{host}} = 0.044$ , and hence obtain a lower value of  $M_{\text{Ni}}$ . The above estimates for iPTF13bvn are lower than the median values for the SN Ib sample ( $M_{\text{ej}} \approx 3.89 M_\odot$ ,  $M_{\text{Ni}} \approx 0.16 M_\odot$ ,  $E_{51} \approx 2.3$  erg), as reported by Cano (2013). Using the estimates provided by B14, the ratio  $E_{51}/M_{\text{ej}} = 0.3$  for iPTF13bvn, lower than the median value of  $0.64 \pm 0.23$  for SNe Ib (Cano 2013).

One way to compare the physical parameters of CCSNe is to plot the  $^{56}\text{Ni}$  mass ( $M_{\text{Ni}}$ ) and kinetic energy ( $E_k$ ) against the estimated main-sequence mass ( $M_{\text{MS}}$ ) of the progenitor (see Nomoto et al. 2006). The estimated progenitor mass for iPTF13bvn is  $\sim 20 M_\odot$  (B14), similar to most normal SNe Ibc. However, the estimated values of  $M_{\text{Ni}}$  and  $E_k$  are similar to those estimated for SNe 1993J and 1994I. Taking a slightly different approach, we plot  $M_{\text{Ni}}$  against the ratio  $E_k/M_{\text{ej}}$  (eg. Bufano et al. 2012) for iPTF13bvn along with a few other CCSNe in the literature (Figure 12). Except for SN 2007Y (Stritzinger et al. 2009) and iPTF13bvn, the values of  $M_{\text{ej}}$ ,  $M_{\text{Ni}}$  and  $E_k$  were taken from Tanaka et al. (2009) and references therein. In the  $M_{\text{Ni}}$  vs  $E_k/M_{\text{ej}}$  diagram, iPTF13bvn lies close to the type IIb SN 1993J and type Ib SN 2007Y. Both SN 1993J (Shigeyama et al. 1994) and SN 2007Y (Stritzinger et al. 2009) were relatively low luminosity events with  $^{56}\text{Ni}$  masses of  $0.08 M_\odot$  and  $0.06 M_\odot$ , respectively, and low estimated progenitor masses of  $\sim 13 M_\odot$ . The progenitor of SN 1993J was part of a binary system (Shigeyama et al. 1994; Woosley et al. 1994, and references therein) and

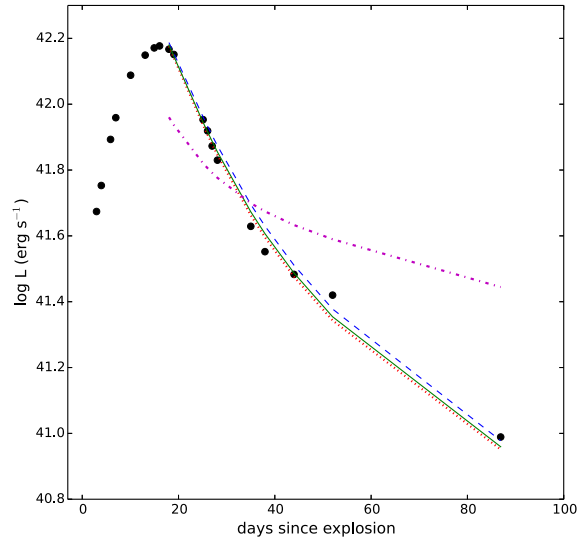


**Figure 11.** Comparison of the observed bolometric light curve of iPTF13bvn with the computed models A, B, C and C1.

underwent mass loss via mass transfer to its companion.

The explosion parameters  $M_{\text{ej}}$  and  $E_k$  arrived at by hydrodynamic modeling (B14, F14), and the estimates provided here are incompatible with a single, massive progenitor with zero age main sequence (ZAMS) mass of  $32 M_\odot$  suggested by Groh et al. (2013). Such a massive star would produce a helium star of  $\sim 8 M_\odot$ , which is too massive to explain the observed properties of the SN (B14). Using hydrodynamic calculations coupled with stellar evolutionary calculations, B14 conclude that the progenitor was a low mass helium star (with a pre-explosion mass of  $\sim 3.5 M_\odot$ ) in a binary system, with an initial configuration of  $20 M_\odot + 19 M_\odot$  and an initial orbit of 4.1 days. Our results favor this model.

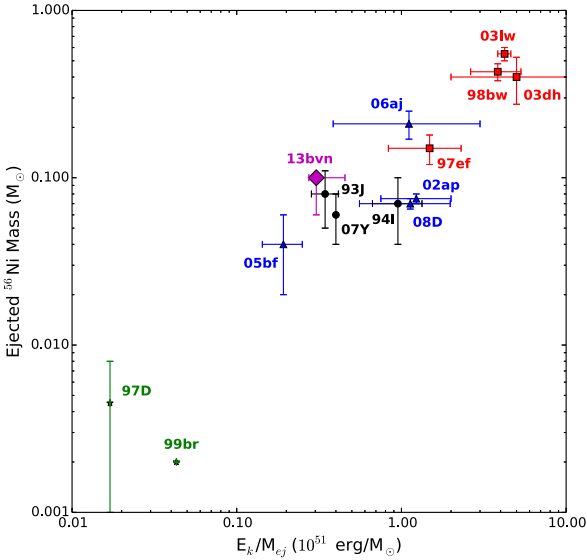
## 9 SUMMARY

The optical light curves of iPTF13bvn show a fast decline ( $\Delta m_{15}(B) = 1.82$ ), which indicates a relatively small ejecta mass. The peak absolute  $V$ -band magnitude,  $V_{\text{max}} = -17.25$  (corrected for  $E(B - V)_{\text{host}} = 0.17$ ) is fainter than the mean extinction-corrected  $V$ -band magnitude of  $-17.9 \pm 0.9$  for the SN Ib sample as reported by Drout et al. (2011). The peak bolometric flux indicates that  $\sim 0.05 - 0.08 M_\odot$  of  $^{56}\text{Ni}$  was synthesized in the explosion, depending upon the adopted value of host reddening. Accounting for a constant 30 % contribution from the UV and NIR passbands, the  $^{56}\text{Ni}$  mass estimate goes up to  $0.06 - 0.09 M_\odot$ .

The optical spectra of iPTF13bvn are marked by an early emergence of the He I 5876 Å feature, identified in the first spectrum taken on day -13. The other features of He I at 4471, 6678 and 7065 Å are weak in the first spectrum but are clearly identified in the spectrum taken on day -6. The photospheric velocity deduced from the

**Table 5.** Parameter values for the computed models fit to the observed bolometric light curve (Vinkó et al. 2004). The asterisk sign indicates fixed parameter values.

Model	$M_{\text{ej}}$ ( $M_{\odot}$ )	$M_{\text{Ni}}$ ( $M_{\odot}$ )	$E_k$ ( $10^{51}$ erg)	$\kappa_{\gamma}$ ( $\text{cm}^2\text{g}^{-1}$ )	$\kappa_{+}$ ( $\text{cm}^2\text{g}^{-1}$ )	$v_{\text{exp}}$ ( $\text{km s}^{-1}$ )	$x_0$	$n$
A	2.2	0.09	1.16	0.008	2.0	12000	1.0*	0.0*
B	1.5	0.09	1.25	0.003	1.0	14000	0.01*	1.2
C	1.6	0.09	0.93	0.005	1.3	12000	0.15*	1.2
C1	2.4	0.05	0.48	0.027*	0.2	9700	0.15*	3.1

**Figure 12.**  $M_{\text{Ni}}$  vs  $E_k/M_{\text{ej}}$  diagram for iPTF13bvn (◆), plotted along with a few literature CCSNe. The parameters for iPTF13bvn are taken from B14, with error bars to accommodate the range of estimates provided in F14 and this work. (■) denotes hypernovae associated with Gamma Ray Bursts (GRBs) with  $E_{51} \gtrsim 10$ , ▲ denotes broad-lined SNe (which includes both GRB and non-GRB SNe), ● represents normal SNe, and ★ represents faint/dark SNe (Nomoto et al. 2006).

Fe II 5169 Å feature is  $\sim 9000 \text{ km s}^{-1}$  near maximum light, being consistent with the average photospheric velocity of  $8000 \pm 2000 \text{ km s}^{-1}$  for SNe Ibc (Cano 2013). The spectra match well with those of the type Ib SN 2009jf, although the light curves are very dissimilar.

Fitting the bolometric light curve with a simple analytical model yields  $M_{\text{Ni}} \sim 0.1 M_{\odot}$ ,  $M_{\text{ej}} \sim 2 M_{\odot}$  and  $E_k \sim 10^{51}$  erg. The narrow peak of the bolometric light curve, and the subsequent fast decline indicates a small ejecta mass, thus being inconsistent with a single, massive Wolf-Rayet progenitor for iPTF13bvn, as pointed out by B14 and F14.

## ACKNOWLEDGEMENTS

We thank the staff of IAO, Hanle and CREST, Hosakote, that made these observations possible. The facilities at IAO

and CREST are operated by the Indian Institute of Astrophysics, Bangalore. We also thank all the HCT observers who spared part of their observing time for the ToO observations. This work has made use of the NASA Astrophysics Data System and the NED which is operated by Jet Propulsion Laboratory, California Institute of Technology, under contract with the National Aeronautics and Space Administration. We thank the anonymous referee for the very positive comments.

## REFERENCES

- Anderson J. P., James P. A., 2008, MNRAS, 390, 1527  
 Anupama G. C., Sahu D. K., Deng J., Nomoto K., Tomimaga N., Tanaka M., Mazzali P. A., Prabhu T. P., 2005, ApJL, 631, L125  
 Arnett W. D., 1982, ApJ, 253, 785  
 Benetti S., Branch D., Turatto M., Cappellaro E., Baron E., Zampieri L., Della Valle M., Pastorello A., 2002, MNRAS, 336, 91  
 Bersten M. C. et al., 2014, ArXiv e-prints  
 Bessell M. S., Castelli F., Plez B., 1998, A & A, 333, 231  
 Branch D. et al., 2002, ApJ, 566, 1005  
 Bufano F. et al., 2012, ApJ, 753, 67  
 Cano Z., 2013, MNRAS, 434, 1098  
 Cao Y., Gorbikov E., Arcavi I., Ofek E., Gal-Yam A., Nugent P., Kasliwal M., 2013a, The Astronomer’s Telegram, 5137, 1  
 Cao Y. et al., 2013b, ApJL, 775, L7  
 Cappellaro E., Mazzali P. A., Benetti S., Danziger I. J., Turatto M., della Valle M., Patat F., 1997, A & A, 328, 203  
 Cardelli J. A., Clayton G. C., Mathis J. S., 1989, ApJ, 345, 245  
 Drout M. R. et al., 2011, ApJ, 741, 97  
 Elmhamdi A., Danziger I. J., Branch D., Leibundgut B., Baron E., Kirshner R. P., 2006, A & A, 450, 305  
 Ensman L. M., Woosley S. E., 1988, ApJ, 333, 754  
 Filippenko A. V., 1997, ARA & A, 35, 309  
 Fisher A. K., 2000, PhD thesis, The University of Oklahoma  
 Folatelli G. et al., 2006, ApJ, 641, 1039  
 Fremling C. et al., 2014, A & A, 565, A114  
 Gaskell C. M., Cappellaro E., Dinerstein H. L., Garnett D. R., Harkness R. P., Wheeler J. C., 1986, ApJL, 306, L77  
 Gilmozzi R. et al., 1987, Nature, 328, 318  
 Groh J. H., Georgy C., Ekström S., 2013, A & A, 558, L1  
 Hunter D. J. et al., 2009, A & A, 508, 371

- Jester S. et al., 2005, *AJ*, 130, 873
- Kelly P. L., Kirshner R. P., Pahre M., 2008, *ApJ*, 687, 1201
- Kirshner R. P., Sonneborn G., Crenshaw D. M., Nassiopoulou G. E., 1987, *ApJ*, 320, 602
- Landolt A. U., 1992, *AJ*, 104, 340
- Lucy L. B., 1991, *ApJ*, 383, 308
- Milisavljevic D. et al., 2013, *The Astronomer's Telegram*, 5142, 1
- Modjaz M. et al., 2009, *ApJ*, 702, 226
- Nomoto K., Tominaga N., Tanaka M., Maeda K., Suzuki T., Deng J. S., Mazzali P. A., 2006, *Nuovo Cimento B Serie*, 121, 1207
- Nomoto K. I., Iwamoto K., Suzuki T., 1995, *Phys. Rep.*, 256, 173
- Nugent P., Branch D., Baron E., Fisher A., Vaughan T., Hauschildt P. H., 1995, *Physical Review Letters*, 75, 394
- Parrent J. et al., 2007, *PASP*, 119, 135
- Podsiadlowski P., Joss P. C., Hsu J. J. L., 1992, *ApJ*, 391, 246
- Richmond M. W. et al., 1996, *AJ*, 111, 327
- Sahu D. K., Gurugubelli U. K., Anupama G. C., Nomoto K., 2011, *MNRAS*, 413, 2583
- Schlaflly E. F., Finkbeiner D. P., 2011, *ApJ*, 737, 103
- Shigeyama T., Suzuki T., Kumagai S., Nomoto K., Saio H., Yamaoka H., 1994, *ApJ*, 420, 341
- Smartt S. J., 2009, *ARA & A*, 47, 63
- Stalin C. S., Hegde M., Sahu D. K., Parihar P. S., Anupama G. C., Bhatt B. C., Prabhu T. P., 2008, *Bulletin of the Astronomical Society of India*, 36, 111
- Stritzinger M. et al., 2002, *AJ*, 124, 2100
- Stritzinger M. et al., 2009, *ApJ*, 696, 713
- Sutherland P. G., Wheeler J. C., 1984, *ApJ*, 280, 282
- Tanaka M. et al., 2009, *ApJ*, 692, 1131
- Thomas R. C., Nugent P. E., Meza J. C., 2011, *PASP*, 123, 237
- Tully R. B., Rizzi L., Shaya E. J., Courtois H. M., Makarov D. I., Jacobs B. A., 2009, *AJ*, 138, 323
- van Dyk S. D., Hamuy M., Filippenko A. V., 1996, *AJ*, 111, 2017
- Vinkó J. et al., 2004, *A & A*, 427, 453
- Woosley S. E., Eastman R. G., Weaver T. A., Pinto P. A., 1994, *ApJ*, 429, 300